Nanoscale Advances

ROYAL SOCIETY OF CHEMISTRY

PAPER

View Article Online
View Journal | View Issue



Cite this: *Nanoscale Adv.*, 2024, **6**, 4417

# Smart photopharmacological agents: $LaVO_4:Eu^{3+}$@vinyl phosphonate combining luminescence imaging and photoswitchable butyrylcholinesterase inhibition†

Gulia Bikbaeva,[a] Anna Pilip,[b] Anastasiya Egorova,[bc] Vasiliy Medvedev,[a] Daria Mamonova,[a] Dmitrii Pankin,[a] Alexey Kalinichev,[a] Natalya Mayachkina,[b] Lyudmila Bakina,[b] Ilya Kolesnikov,[a] Gerd Leuchs *[d] and Alina Manshina *[a]

The combination of photoswitchability and bioactivity in one compound provides interesting opportunities for photopharmacology. Here, we report a hybrid compound that in addition allows for its visual localization. It is the first demonstration of its kind and it even shows high photoswitchability. The multifunctional nanomaterial hybrid, which we present, is composed of luminescent $LaVO_4:Eu^{3+}$ nanoparticles and vinyl phosphonate, the latter of which inhibits butyrylcholinesterase (BChE). This inhibition increases 7 times when irradiated with a 266 nm laser. We found that it is increased even further when vinyl phosphonate molecules are conjugated with $LaVO_4:Eu^{3+}$ nanoparticles, leading in total to a 20-fold increase in BChE inhibition upon laser irradiation. The specific luminescence spectrum of $LaVO_4:Eu^{3+}$ allows its spatial localization in various biological samples (chicken breast, Daphnia and Paramecium). Furthermore, laser irradiation of the $LaVO_4:Eu^{3+}$@vinyl phosphonate hybrid leads to a drop in luminescence intensity and in lifetime of the $Eu^{3+}$ ion that can implicitly indicate photoswitching of vinyl phosphonate in the bioactive state. Thus, combining enhanced photoswitchability, bioactivity and luminescence induced localizability in a unique way, hybrid $LaVO_4:Eu^{3+}$@vinyl phosphonate can be considered as a promising tool for photopharmacology.

Received 9th May 2024
Accepted 20th June 2024

DOI: 10.1039/d4na00389f

rsc.li/nanoscale-advances



## 1. Introduction

Photopharmacology is a breakthrough trend in modern medicine. It is based on using light to selectively activate or deactivate drugs in a given area of the body and at a given period.[1,2] The concept of photopharmacology has revolutionized the classical therapeutic approach and suggested novel treatment strategies for numerous diseases. The most promising breakthrough of photopharmacology is expected in oncology, neuroscience, and ophthalmology. The main advantage of photopharmacology is the optimized duration of therapy and its precise targeting to specific areas of the body, thus reducing the amount of drug and side effects, and minimizing collateral damage to surrounding tissues and environmental burden.

The main achievement of modern photopharmacology is the creation of photosensitive drugs obtained by incorporation of light-responsive moieties into the structure of drugs. Light-responsive molecules or photoswitches are molecules existing as two or more isomers with the possibility of switching between isomeric states by means of light irradiation.[3] The change in molecule conformation under light stimulus can take place *via* rotation, dynamic bond cleavage, cyclization, double-bond isomerization, *etc.*[2,4] As photoswitches, families of azo compounds, stilbenes, and diarylethenes are mainly used.[2] As variants of drugs, antibiotics (vancomycin, cephalosporin, gramicidin, and diaminopyrimidines) and anti-Alzheimer's medicine Tacrine were demonstrated.[5–9] A similar strategy for imparting photosensitivity to medicinal compounds is 'azologization' (azobenzene + analogization), allowing the creation of photochromic azoderivatives of drugs.[10,11] Thus, the use of different variants of reversible or irreversible photoswitches (switching 'on', 'off', or 'on/off') allowed the creation of photopharmacological agents for various therapeutic scenarios: irradiation prior to administration, irradiation at the point of action, multiple irradiation cycles of a drug, *etc.*[2]

[a]*St Petersburg State University, 7-9 Universitetskaya Embankment, St Petersburg, 199034, Russia. E-mail: a.manshina@spbu.ru*

[b]*St Petersburg Federal Research Center of the Russian Academy of Sciences (SPC RAS), Scientific Research Centre for Ecological Safety of the Russian Academy of Sciences, Korpusnaya 18, St Petersburg, 197110, Russia*

[c]*St Petersburg State Technological Institute (Technical University), 26, Moskovski Ave., St Petersburg, 190013, Russia*

[d]*Max Planck Institute for the Science of Light, Erlangen, 91058, Germany. E-mail: gerd.leuchs@mpl.mpg.de*

† Electronic supplementary information (ESI) available. See DOI: https://doi.org/10.1039/d4na00389f

It should be noted that the special attention of photopharmacology is focused on treatment of diseases related to a family of important enzymes – acetylcholinesterase (AChE) and butyrylcholinesterase (BChE). These esterases participate in neuronal transmission and can be connected with serious human disorders such as Alzheimer's disease, memory disorders, numerous skin diseases, *etc.*[12–15] It was demonstrated that photopharmacology can offer photoswitchable AChE and BChE inhibitors promising for the efficient treatment of the listed problems.[5,16,17] Therefore, the potency of photopharmacology was successfully confirmed by the achievements of several scientific groups in their publications that demonstrate experiments *in vitro*[18,19] and even *in vivo*.[1,20–23]

However, a highly requested function of visualization of photopharmacological drug localization in biological tissues is still unrealized. One of the main reasons for this lack is the following. The creation of a photosensitive medicinal compound by a traditional approach – the conjunction of a photoswitch and drug – is an extremely labor-intensive process. The key requirement for photoswitchable drugs is a pronounced difference in bioactivity between isomeric states before and after laser irradiation. However, a drug is typically optimized to provide the necessary therapeutic effect. Conjunction of a drug with a photoswitch usually leads to a loss or decrease in the bioactivity of the 'drug + photoswitch' compound compared to the initial drug. Therefore, imparting additional luminescent properties to the compound 'drug + photoswitch' in conjunction with the third component – the luminescent species, will lead to loss or disturbance of bioactive and photoswitchable properties. Thus, the construction of a three-component compound possessing 'drug + photoswitch + luminescence' properties is a formidable problem. Currently, only groups of substances obtained by a combination of 2 compounds with 'bioactive and photoswitching' or 'photoswitching and luminescence' or 'bioactive and luminescence' properties have been reported.[24–30]

To the best of our knowledge, there is the only publication demonstrating hybrid nanomaterial carbon quantum dot@-phosphonate having three functions important for photopharmacology simultaneously: bioactivity; photoswitching; luminescence.[31] The creation of such a multifunctional hybrid was possible due to a new group of phosphonate compounds that join functions of butyrylcholinesterase inhibition and photoisomerization.[32–34] Thus, the conjunction of only two components – the photoswitchable bioactive phosphonate with carbon quantum dots (CQDs) famous for their luminescence provided a 'drug + photoswitch + luminescence' hybrid nanomaterial. It should be noted that the creation of hybrids based on new photoswitchable phosphonates and various carriers such as fullerenes and CQDs allows not only to maintain bioactivity, but also to improve the bioactivity difference between isomeric states before and after laser irradiation.[31,35]

It is well known that luminescence properties (intensity, spectral position, and lifetime) of CQDs are extremely sensitive to the environment.[36] They can be considered as an efficient sensing features of CQDs and hybrids on their base. However, stability of the luminescence parameters in various media, including biological tissues, is a critical characteristic for solving tasks of spatial visualization of photopharmacological agents. That is why motivation for the current research was the creation of a photoswitchable bioactive hybrid with stable luminescence properties (spectral position) for visualization of the localization in different biological objects, and unambiguous detectability against the autofluorescence of biological tissues.

Metal oxide nanoparticles (NPs) doped with rare earth ions (REIs) are well-known objects providing luminescence bands with spectral positions clearly defined by exact REIs. REI-doped materials are characterized by large pseudo-Stokes shifts, narrow emission bands, long lifetimes and high photostability revealing no luminescence blinking or degradation in time.[37–39] Thanks to the rational choice of doping REIs, one can detect their luminescence against the background of autofluorescence typical for biological tissues.[40] Moreover, oxide nanoparticles are biocompatible and can be used as components of theranostic compounds.[41–43]

Here, we report the first hybrid organic–inorganic nanomaterial $LaVO_4$:$Eu^{3+}$@vinyl phosphonate (hereafter **LEu@VP**) that can be considered as a photopharmacological agent with advanced features – luminescence imaging and photoswitchable bioactivity. Here, $LaVO_4$:$Eu^{3+}$ 2 at% NPs (**LEu**) act as a luminescence center and carrier for photoswitchable bioactive vinyl phosphonate – di(prop-2-yl)[(*Z*)-2-chloro-2-phenylethenyl] phosphonate (**VP**). The choice of $Eu^{3+}$ as a doping ion is justified by abundant emission lines and strong luminescence, whereas the $LaVO_4$ crystalline host is chosen because of its chemical and thermal inertness as well as low point symmetry ($C_1$) around the substitution site resulting in intense emission intensity.[44,45]

Di(prop-2-yl)[(*Z*)-2-chloro-2-phenylethenyl] phosphonate belongs to the family of vinyl phosphonates demonstrated earlier.[46] The important peculiarity of the chosen **VP** is good inhibition of butyrylcholinesterase (the inhibition constant $C_i$ = 0.0037 $\mu M^{-1}$ $min^{-1}$), and strong inhibition increase – from 10% to 90% for $10^{-6}$ M after laser illumination with wavelength 266 nm.[34] Such a strong inhibition change was attributed to *cis–trans* photoisomerization by the C=C bond with a quantum yield of 20%.

The novelty of the research is the demonstration of $LaVO_4$:-$Eu^{3+}$@vinyl phosphonate hybrids with advanced properties promising for photopharmacology – photoluminescence imaging and 'switching on' of BChE inhibition. The characteristic luminescence bands typical for $Eu^{3+}$ ions make the **LEu@VP** hybrid promising for visualization of spatial localization in biological models such as Daphnia and Paramecium, and the possibility of luminescence detection against the autoluminescence of biotissues using a chicken breast as an example.

## 2. Materials and methods

### 2.1. Synthesis of di(prop-2-yl)[(*Z*)-2-chloro-2-phenylethenyl] phosphonate

Phenylacetylene (reagent grade, ≥97%, Sigma-Aldrich), benzene (Pure, Lenreaktiv, St. Petersburg, Russia), and

 

isopropyl alcohol (Pure, Lenreaktiv, St. Petersburg, Russia) were purified *via* standard methods before use and handled under an atmosphere of nitrogen. Potassium carbonate (anhydrous, reagent grade, ≥98%, powder, −325 mesh, Sigma-Aldrich) and phosphorus pentachloride (Pure, LLC JSC "REAKHIM", St. Petersburg, Russia) were also used in the synthesis process.

Di(prop-2-yl)[(*Z*)-2-chloro-2-phenylethenyl] phosphonate (**VP**) has been synthesized according to a protocol reported earlier.[46] The reaction progress monitoring was carried out by using $^{31}$P NMR spectra. The final product is a yellow oily liquid, readily soluble in polar organic solvents. The $^{31}$P NMR chemical shift of phosphonate was observed in a field at 10.73 ppm. NMR spectra were recorded in $CDCl_3$ on a Bruker Avance III HD 400 NanoBay spectrometer at frequencies of 400.17 ($^1$H), 100.62 MHz ($^{13}$C), and 161.98 MHz ($^{31}$P).

The structure of the synthesized **VP** is presented in Fig. 1.

### 2.2. Synthesis of $LaVO_4$:$Eu^{3+}$ particles

Lanthanum oxide ($La_2O_3$, 99.995%), europium oxide ($Eu_2O_3$, 99.999%) and vanadium oxide ($V_2O_5$, 98.5%) were utilized as starting materials for the synthesis of $LaVO_4$:$Eu^{3+}$ particles. Europium and lanthanum oxides were converted to nitrate by adding concentrated nitric acid (70% $HNO_3$). Citric acid ($C_6H_8O_7$, 99.8%), ethylene glycol ($C_2H_6O_2$, 98.5%) and potassium chloride (KCl, 99.8%) were also used in the synthesis process.

$LaVO_4$:$Eu^{3+}$ particles have been synthesized *via* the modified Pechini method described in detail earlier.[44] Metal citrate complexes were prepared according to the following reactions:

$$La(NO_3)_3 + 3C_6H_8O_7 = [La(C_6H_8O_7)_3](NO_3)_3 \quad (1)$$

$$Eu(NO_3)_3 + 3C_6H_8O_7 = [Eu(C_6H_8O_7)_3](NO_3)_3 \quad (2)$$

$$V_2O_5 + 5C_6H_8O_7 = 2VO(C_6H_7O_7)_2 + 6CO + 2H_2O + 4H_2 \quad (3)$$

Ethylene glycol was used to prepare the polymer gel, which was then calcined in two stages. The first heat treatment stage at 600 °C for 2 hours is used to remove organic compounds. The powder was then co-dispersed with potassium chloride or sodium sulfate in a mass ratio of 1 : 1. The second stage was carried out in salt melt at 900 °C for 1 hour. The salt was removed from the product by washing it in distilled water. The $LaVO_4$:$Eu^{3+}$ 2 at% sample was synthesized according to the method described above.

### 2.3. Synthesis of hybrids $LaVO_4$:$Eu^{3+}$@vinyl phosphonate

Colloidal solutions of particles were obtained by dispersing the synthesized $LaVO_4$:$Eu^{3+}$ powders with an ultrasonic homogenizer (UP400S, Hieischer Ultrasonics, 24 kHz, 400 W) in dichloromethane or distilled water for 3 minutes. The coarse fraction (the fraction of microsized particles) was separated by centrifugation for 3 minutes (Sigma 2-16P, 1000 rpm). The final concentration of solutions of nanosized particles was 0.3 g $L^{-1}$. Hybrids **LEu@VP** were synthesized by mixing of the initial components – colloid solution of $LaVO_4$:$Eu^{3+}$ NPs in dichloromethane and of di(prop-2-yl)[(*Z*)-2-chloro-2-phenylethenyl] phosphonate. 25 μL of **VP** was added to 975 μL of colloidal solution of **LEu** in dichloromethane. Hybrids were prepared by mixing the components under ambient conditions with a magnetic stirrer for 1 hour at room temperature (22 °C).

### 2.4. Photoluminescence spectroscopy

The steady-state photoluminescence spectra were collected using a modular spectrofluorometer Fluorolog-3 (Horiba, Japan) with a continuous wave Xe lamp ($P$ = 450 W) as an

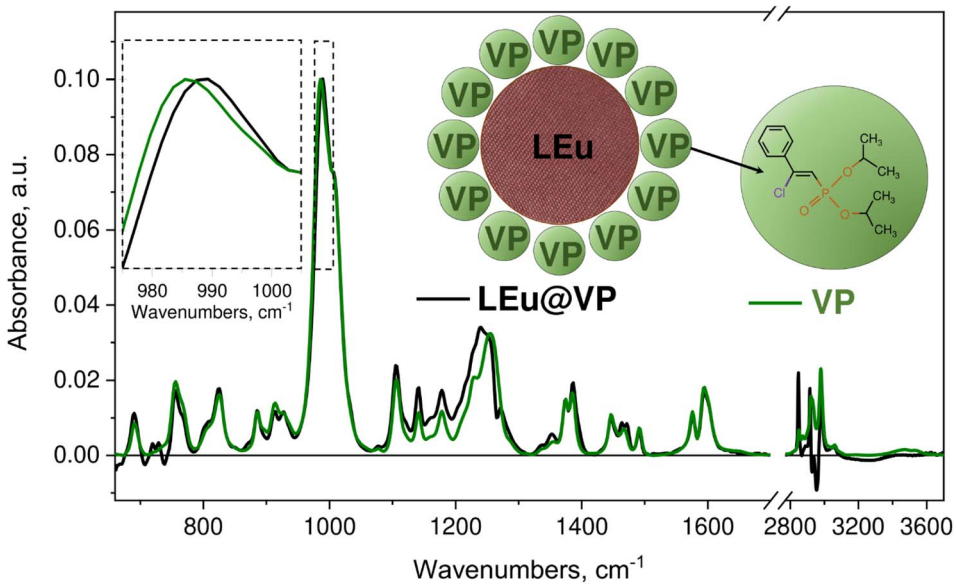


Fig. 1 Schematic representation of hybrids **LEu@VP** and absorbance spectrum of **VP** solution in dichloromethane with subtraction of solvent contribution (green) and absorbance spectrum of hybrids **LEu@VP** solution in dichloromethane with subtraction of solvent and **LEu** contributions (black).

excitation source. Luminescence kinetic measurements were performed using the same spectrofluorometer with a pulsed Xe lamp ($P = 150$ W, pulse width 3 μs). The photoluminescence quantum yield was measured *via* the absolute method using an integrating sphere Quanta-φ. The excitation intensities used for steady-state and kinetic photoluminescence measurements were very low and did not affect the samples. Formalin-fixed Daphnia and Paramecium specimens were imaged using a Nikon Eclipse Ti2 confocal inverted fluorescence microscope (Nikon Corporation, Tokyo, Japan) using a ×40 water-immersion objective. The luminescence of the samples was excited by using a laser with a wavelength of 405 nm and recorded in the spectral range of 520–710 nm using a spectral 32-channel detector with a resolution of 6 nm.

### 2.5. FTIR absorption spectroscopy

The IR absorbance spectra were obtained using a Nicolet8700 (Thermo Scientific, Waltham, MA, USA) using an ATR accessory with a diamond crystal in the 650–4000 $cm^{-1}$ range. The resolution was 4 $cm^{-1}$. The number of scans was 100. The detector was MCT-A with liquid $N_2$ cooling. The beam splitter was XT-KBr. The Blackman-Harris apodization function was chosen. The phase correction was performed according to the Mertz technique. To study the interaction of a phosphonate molecule with NPs, FTIR spectra of **VP** in dichloromethane and hybrids **LEu@VP** in dichloromethane were recorded. Then the solvent contribution was subtracted, and **VP** and hybrids **LEu@VP** difference spectra were compared and discussed in the Results section. The details of the spectral treatment are presented in ref. 31. The spectrum processing was performed in the Origin 9 software (OriginLab Co., Northampton, MA, USA).

### 2.6. BChE activity measurements

Butyrylcholinesterase from horse blood plasma (EC 3.1.1.8), activity 264 U $mg^{-1}$ (Sigma-Aldrich), bovine serum albumin (BSA) (Sigma-Aldrich), butyrylthiocholine chloride (Sigma-Aldrich); HEPES buffer solution (HEPES 0.005 M + KCl 0.003 M, pH 7.5) (Sigma-Aldrich); $KMnO_4$, and $Mn(Ac)_2 \times 4H_2O$, $K_2CO_3$ (anhydrous, reagent grade, ≥98%, powder, −325 mesh, Sigma-Aldrich) were used for measurements of biological activity.

Butyrylcholinesterase (BChE) activity was calculated from the initial rate of biocatalytic hydrolysis of butyrylthiocholine, which was determined from the accumulation of thiocholine using a thiol-sensitive sensor. The reaction to thiocholine which occurred during the enzymatic hydrolysis of butyrylthiocholine was recorded in the product accumulation mode (Scheme 1). BChE activity before and after inhibition was measured using an amperometric neurotoxin analyzer IPC-micro EasyCheck-Micro (Kronas, Russia) with planar electrodes modified with $MnO_2$ (BVT, Czech Republic).

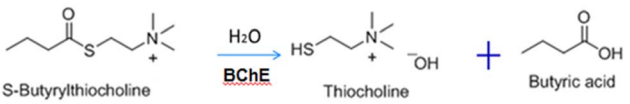


Scheme 1 Enzymatic hydrolysis of butyrylthiocholine with the formation of electrochemically active thiocholine.

First, a blank experiment to determine BChE activity – the $A_0$ value, and BChE activity in the presence of solvent dichloromethane – $A_{0c}$ was carried out. Then the measurements of BChE inhibition were carried out for initial (**VP** and **LEu@VP**) and laser-irradiated samples (**VP-LI** and **LEu@VP-LI**). The necessary amount of sample was added to the system with BChE. The residual BChE activity values after inhibition by the studied samples ($A$) were determined and normalized by using $A_{0c}$. The inhibition was calculated as $A_{0c}/A$ 100%. All the measurements were carried out 5 times.

### 2.7. Laser irradiation of the samples

Laser irradiation of the samples was performed with a Coherent MBD 266 solid-state laser (Santa Clara, CA, USA) (continuous wave, $\lambda = 266$ nm, power 60 mW) with a defocused laser beam ($d = 10$ mm) in a 1 cm thick quartz cell. The laser irradiation time was 60 min in all these experiments.

### 2.8. Testing of hybrid LEu@VP luminescence on biological models

3 model bioobjects such as the samples of a chicken breast, crustacean *Daphnia magna* str., and protozoan *Paramecium caudatum* Her. were chosen for luminescence visualization of $LaVO_4$:$Eu^{3+}$. Chicken breast samples were bought at the market; crustacean *Daphnia magna* str., and protozoan *Paramecium caudatum* Her. were genetically homogeneous laboratory cultures from the collection of the Scientific Research Centre for Ecological Safety of the Russian Academy of Sciences. As a model experiment with a complex biological sample with autofluorescence, a cut-out piece of chicken breast (across muscle fibers) was used. Hybrids **LEu@VP** were injected with a syringe into the chicken breast to a depth of *ca.* 0.5 mm. Part of the substance was poured onto the surface of the chicken breast; then the surface was carefully blotted with fat-free napkins.

To study spatial distribution and possibility of luminescence visualization, 10 2 day-old Daphnia or 1 mL of Paramecium culture were placed in a test tube with a colloidal solution of $LaVO_4$:$Eu^{3+}$ NPs in water. The volume of the colloidal solution was 50 mL for Daphnia and 10 mL for Paramecium. Control test organisms were placed in clean water. Containers with control and test organisms were placed in a cassette rotating at a speed of 6–8 rpm for continuous and uniform mixing of nanoparticle solutions, safe for living test objects. The experiment was repeated three times. The duration of the stay of organisms in solutions was 24 hours.

After the end of the exposure, the experimental organisms were washed from nanoparticles. For this purpose, Daphnia were sequentially placed in two glasses of distilled water with a volume of 100 mL for 10 seconds each. To wash the Paramecium, the reaction of moving (floating) Paramecium to the upper part of the liquid was used. When Paramecium are placed in narrow-necked flasks, they are accumulated in the upper 1–2 cm layer of liquid and can be compactly drained in a minimal

 

amount of solution. Therefore, to wash the Paramecium, they were placed twice successively in narrow-necked flasks with a volume of 100 mL for 30 minutes each, after which they were poured into a clean glass. After the washing procedure, the test organisms were preserved with a 3.7% formaldehyde solution in 40% ethanol.

## 3. Results and discussion

### 3.1. Characterization of hybrids LEu@VP

Vinyl phosphonate (**VP**) and luminescent nanoparticles $LaVO_4$:-$Eu^{3+}$ (**LEu**) were used as component parts for the synthesis of hybrids **LEu@VP**. The structure, morphology and luminescent properties of $LaVO_4$:$Eu^{3+}$ nanoparticles were studied using XRD, SEM and photoluminescence spectroscopy. The XRD analysis shows diffraction lines for the monoclinic modification of $LaVO_4$ with the $P2_1/n$ space group (Fig. S1a†). The synthesized particles exhibit a well-formed crystal structure and exist as a single phase. Statistical analysis of the SEM image shows that the powder contains particles with an average size of (130 ± 20) nm (Fig. S1b†). **LEu** demonstrates typical narrow lines in both excitation and emission spectra corresponding to the 4f–4f intra-configurational transitions inside $Eu^{3+}$ ions[47] (Fig. S2†). The photoluminescence quantum yield of **LEu** was found to be 9%. More detailed discussion is provided in the ESI.†

The synthesis of hybrids **LEu@VP** was based on the physisorption of **VP** molecules on the surface of **LEu** nanocrystalline particles. The hybrid was prepared by mixing the components under ambient conditions for 1 hour. The schematic representation of hybrids **LEu@VP** is shown in Fig. 1. **LEu@VP** hybrid formation and **VP** interaction with **LEu** were confirmed with FTIR spectroscopy. Fig. 1 demonstrates the absorbance difference spectrum of **VP** with the subtracted contribution of the solvent. The FTIR spectrum of **VP** is characterized by several peaks attributed to the $\nu_{as}(CH_3)$ (2984 $cm^{-1}$), $\nu$(C=C) (1594 and 1575 $cm^{-1}$), v19a in **VP** according to Wilson notations (1445 $cm^{-1}$), P=O, $\delta$(HCC) (1254 $cm^{-1}$), mainly $\nu$(C–O) (986 $cm^{-1}$), v12 in Ph, $\delta$(PCC), $\delta$(CCC) (913 $cm^{-1}$), mainly $\nu$(CP) (828 $cm^{-1}$), and out of plane vibration (HCCC) (754 $cm^{-1}$). One can observe some shift of the absorbance peaks for the **VP** dichloromethane solution compared to the undissolved **VP** presented in ref. 46. The most significant shift is observed for vibration modes including polar groups assigned to $\nu$(P=O) and $\delta$(HC=C) (1247 to 1254 $cm^{-1}$), as well as $\nu$(C–O) (1017 to 986 $cm^{-1}$) for undissolved **VP** and **VP** dichloromethane solution respectively. Thus, the peaks associated with the phosphonate and vinyl parts can be considered to be sensitive to the environment and promising for the analysis of **VP** interaction with **LEu**.

On comparing **VP** and hybrid **LEu@VP**, the most significant changes between the two spectra in Fig. 1 occur in the 1100–1265 $cm^{-1}$ region associated with phosphonate and vinyl parts of the **VP** molecule. The maximum of the 1200–1265 $cm^{-1}$ band shifts from the frequency of 1254 $cm^{-1}$ in the case of the **VP** sample to 1238 $cm^{-1}$ in the case of the hybrid sample, whereas the $\nu$(C–O) peak demonstrates a 4 $cm^{-1}$ upshift. Thus, the obtained results reveal the interaction between **LEu** and **VP** through the polar P=O bond and the H–C= of the vinyl part. It should be noted that hybrid formation *via* the phosphonate group is typical for the family of phosphonate compounds.[31,35]

### 3.2. Laser irradiation and characterization of hybrids LEu@VP

Hybrid **LEu@VP** was proposed as a photopharmacological agent; therefore, the pharmacological properties and their changes under the light stimulus were studied in detail. Biological activity of **VP**, **LEu**, and hybrids **LEu@VP** as well as the corresponding laser-irradiated samples (**VP-LI**, **LEu-LI**, and **LEu@VP-LI**) was estimated by measuring BChE inhibition. **LEu** colloidal solution in dichloromethane was found to show a trace inhibition of approximately 10%. Inhibition of **VP** was found to be 12% for a concentration of $10^{-6}$ M, whereas hybrids **LEu@VP** do not show BChE inhibition (Fig. 2).

To study the effect of laser irradiation on bioactive properties, the dichloromethane solution of hybrids **LEu@VP** was irradiated by using a laser with a wavelength of 266 nm, I ~60 mW $cm^{-2}$ for 60 min. Blank experiments on laser irradiation of dichloromethane solution of **VP** and **LEu** with the same parameters were carried out for comparison (the samples **VP-LI**

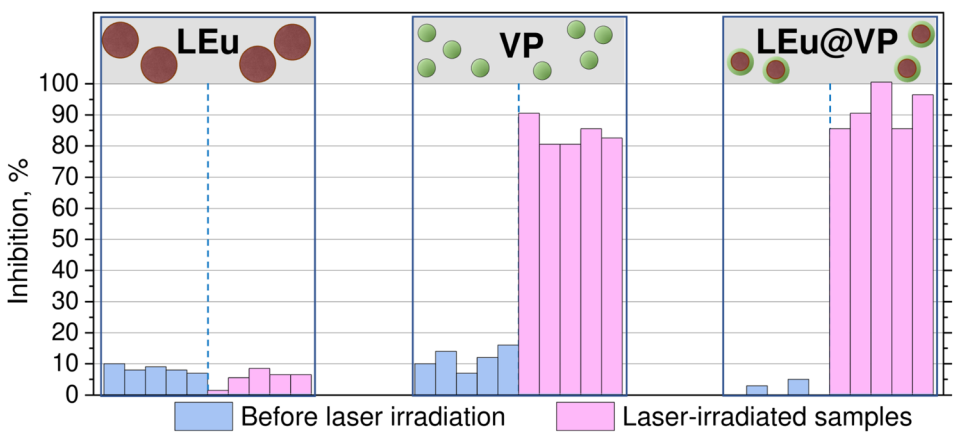


Fig. 2 BChE inhibition for **LEu**, **VP**, Hybrids **LEu@VP** and laser-irradiated samples **LEu-LI**, **VP-LI** and **LEu@VP-LI**. Data repeatability was checked for five samples.

and **LEu-LI,** respectively). As expected, laser irradiation does not affect **LEu** bioactivity. However, BChE inhibition by **VP-LI** is 85% which is 7 times higher than that of **VP**. A more significant increase in the difference in the BChE inhibition was detected for hybrids **LEu@VP** (4%) and hybrids **LEu@VP-LI** (92%). One can see the BChE inhibition increase by almost an order of magnitude – more than 20 times.

### 3.3. Luminescence properties of hybrids LEu@VP

Emission spectra of **LEu**, hybrids and hybrids after laser irradiation are presented in Fig. 3a. Spectra of all samples contain typical $Eu^{3+}$ characteristic transitions from metastable $^5D_0$ to ground $^7F_J$ ($J = 1$–4) levels. Luminescence intensity of hybrids **LEu@VP** is slightly lower compared to that of pure $LaVO_4$:$Eu^{3+}$ nanoparticles, whereas laser-irradiated hybrid **LEu@VP-LI** significantly reduces emission by more than 100 times.

In addition to steady-state luminescence, an effect of hybrid formation and laser irradiation has been studied by luminescence kinetic measurements. Fig. 3b shows decay curves monitored at the $^5D_0$–$^7F_2$ transition for all samples. Experimental data were fitted by using a single exponential function: $I = I_0 \cdot e^{-\frac{t}{\tau_f}}$, where $\tau_f$ is the observed lifetime of the $^5D_0$ level. It can be seen that **LEu** and Hybrids **LEu@VP** have a similar lifetime of ~1.3 ms, while the lifetime of the hybrid sample after irradiation, **LEu@VP-LI,** demonstrates a noticeable reduction down to ~0.4 ms (Fig. 3c). A strong drop in luminescence intensity and observed lifetime as a result of laser irradiation can probably be elucidated *via* the change in nonradiative decay rates. According to our previous study, **VP** undergoes *cis–trans* isomerization upon laser irradiation.[34] Thus, it can be assumed that such *cis–trans* isomerization of **VP** on the surface of $LaVO_4$:$Eu^{3+}$ nanoparticles could significantly enhance the nonradiative decay rate.

### 3.4. Testing of hybrid LEu@VP functionality and luminescence imaging on biological models

Controlling the location of drugs in organs and tissues of the body is a fundamental factor in the treatment of a wide list of localized diseases (skin diseases and ophthalmic problems) or diseases that require site-specific drug delivery (Alzheimer's, myocardial infarction, oncological diseases, *etc.*).[31] To visualize drug localization, luminescent labels can be applied. Successful implementation of the luminescent labels requires tackling the problem of autofluorescence intrinsic properties of cells and biological tissues. Thus, a study of the possibility of detecting a luminescent label against the background of autofluorescence is an essential test for biomedical applicability. Another important task is the control of spatial localization of luminescent labels in the case of their inhomogeneous distribution in biosamples.

Visualization of NP localization in biological samples was studied for 3 model bioobjects such as – a sample of a chicken breast, crustacean *Daphnia magna* str., and protozoan *Paramecium caudatum* Her. The choice of model samples was determined by the following factors: the chicken breast sample is a rather complex model close to real tissues for photopharmacology. The chicken sample is characterized by typical autofluorescence for biotissues. Thus, it allows studying the detectability of hybrids **LEu@VP** luminescence against autofluorescence of the chicken breast sample. Daphnia and protozoa Paramecium were chosen to demonstrate the penetration of nanoparticles into biosamples and the spatial distribution study by luminescence control.

The experiment with a chicken sample was carried out for solution of hybrids **LEu@VP** in dichloromethane, whereas Daphnia and Paramecium experiments were carried out with **LEu** water solution.

As a biological model in our *ex vivo* experiment, a cross section cut out of a chicken breast (across muscle fibers) was prepared. 20 mL of colloidal solutions of **LEu**, hybrids **LEu@VP**, and hybrids **LEu@VP-LI** were injected with an insulin syringe under the sample surface *ca.* 0.5 mm. Fig. 4a shows the luminescence of hybrids **LEu@VP** and their localization in the sample. The comparison of luminescence of **LEu**, initial **LEu@VP** and irradiated **LEu@VP-LI** hybrids measured for the chicken breast sample is presented in Fig. 4b. **LEu** and initial **LEu@VP** display intense characteristic emission lines situated in the orange and red spectral range upon UV excitation. One can see that bybrids **LEu@VP** have just slightly less emission

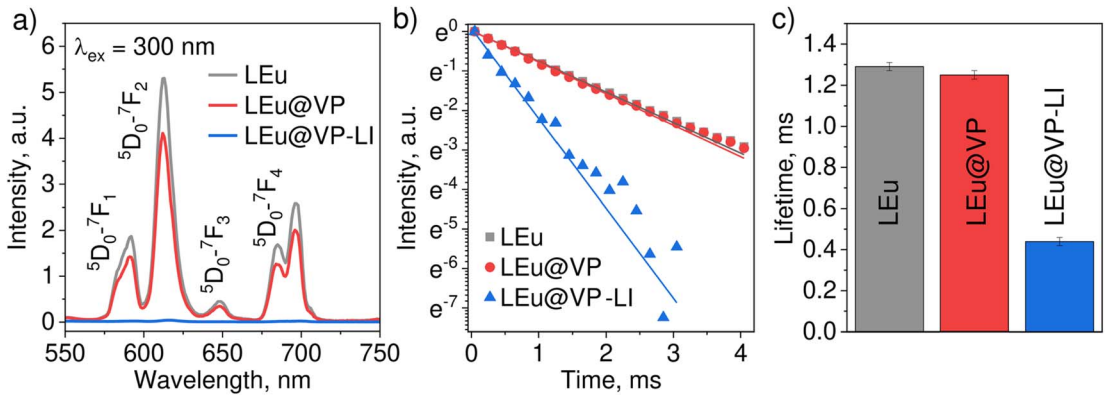


Fig. 3 Luminescence characterization of **LEu**, hybrids **LEu@VP**, and laser-irradiated hybrid **LEu@VP-LI**: (a) emission spectra, (b) luminescence decay, and (c) lifetimes.

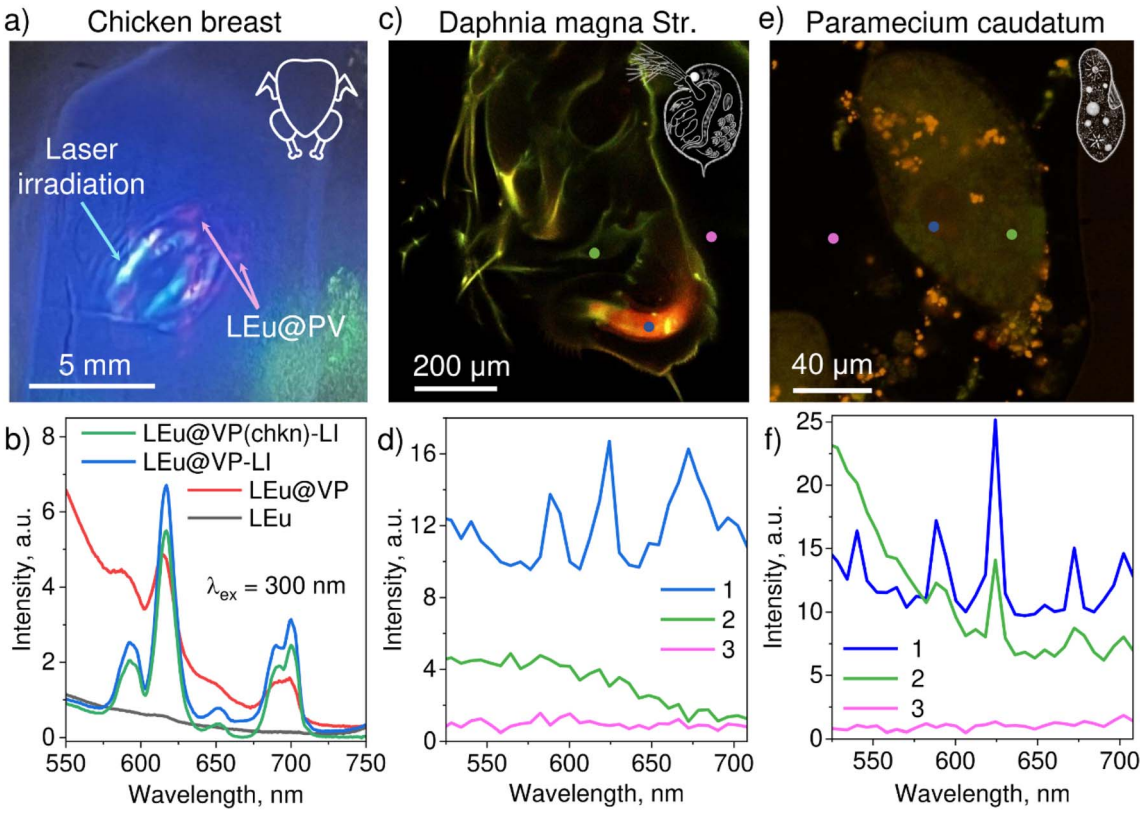


Fig. 4 Luminescence imaging for (a) the chicken breast sample, (b) luminescence spectra of LEu, LEu@VP and LEu@VP-LI hybrids measured in the chicken breast and LEu@VP(chkn)-LI measured as LEu@VP irradiated in chicken (c) crustacean *Daphnia magna* str., (d) luminescence spectra of LEu measured in different areas of *Daphnia magna*, (e) protozoan *Paramecium caudatum* Her, and (f) luminescence spectra of LEu measured in different areas of *Paramecium caudatum* Her.

compared to **LEu**. As previously, laser-irradiated hybrid **LEu@VP-LI** demonstrates a significant drop in emission intensity; however, a weak band at 615 nm is still visible in the spectrum. The line width and large spectral separation from the excitation wavelength make these phosphors potential candidates for photoluminescence bioimaging.

To check the possible laser treatment of the photopharmacological agent inside biological tissue, initial hybrid **LEu@VP** was injected under the surface of the chicken sample, and was further irradiated with an unfocused 266 nm laser with a power of 40 mW for 30 minutes (Fig. 4b). This sample is called **LEu@VP(chkn)-LI**. It can be seen that such laser treatment results in a decrease in emission intensity. A smaller drop in the intensity of **LEu@VP(chkn)-LI** in comparison with hybrids **LEu@VP-LI** can be explained by the absorption of laser radiation by biological tissue. However, luminescence of **LEu** is unambiguously detectable against the autofluorescence of biological tissue thanks to the specific characteristics of the excitation and luminescence bands of $Eu^{3+}$ ions.

The possibility of visualization of hybrid localization in biological samples was also studied for model bioobjects such as crustacean *Daphnia magna* str. and protozoan *Paramecium caudatum* Her. The aim of the experiment was the investigation of the possibility of **LEu** penetration into the bioobject, and visualization of spatial localization based on luminescence control. The saturation of the bioobjects with **LEu** was carried out by the procedure described in the Methods section. It was found that experiments with Daphnia provide a clear distribution of **LEu** mainly in the digestive system, which is confirmed by typical emission spectra for $Eu^{3+}$ (Fig. 4c and d, area 1). Area 2 of Daphnia and area 3 (control zone outside Daphnia) do not show luminescence. The Paramecium bioobject does not demonstrate specific distribution of **LEu**. Thus, the luminescence signal is detectable in the macronucleus and digestive vacuoles (Fig. 4e and f, areas 1 and 2). It should be noted that the Paramecium sample demonstrates many agglomerated NPs on the surface that are highly likely detained by cilia.

## 4. Conclusions

In this work we presented for the first time an organic–inorganic hybrid nanomaterial combined with luminescent $LaVO_4$:$Eu^{3+}$ nanoparticles surrounded by the organic shell of di(prop-2-yl)[(*Z*)-2-chloro-2-phenylethenyl] phosphonate. The core–shell interaction of the hybrid was confirmed by FTIR spectroscopy and revealed through the polar P=O bond and the H–C= of the vinyl part of **VP**. The produced **LEu@VP** hybrid was demonstrated as a compound, which is at the same time simultaneously luminescent, bioactive, and photoswitchable. The luminescent properties of the hybrid are similar to that of

**LEu** NPs. **LEu@VP** hybrid bioactivity shows BChE inhibition typical for **VP**. It is worth noting that the hybrid not only retains the ability to increase BChE inhibition under laser irradiation with a wavelength of 266 nm by analogy with **VP**, but is also characterized by a larger increase in bioactivity (4% to 92%) compared to pure **VP** (12 to 85%). Luminescence characterization of the laser-irradiated **LEu@VP-LI** hybrid demonstrated the preservation of the spectral position of luminescence bands with a simultaneous significant decrease in the intensity and lifetime of luminescence. The specific luminescence spectrum of the **LEu** NPs allows their spatial localization in various biological samples (chicken breast, Daphnia and Paramecium) as it is well detectable against the autofluorescence of biological tissues (chicken breast as an example). Favorably combining the three functions bioactivity, luminescence imaging and photoswitchable butyrylcholinesterase inhibition offers interesting opportunities for pharmacology.

## Data availability

All experimental data for this study are included in this published article and its ESI.†

## Author contributions

G. B., V. M., N. M., L. B., and A. K. performed the experimental work. A. P., A. E., and D. P. performed the experimental work and wrote the manuscript. M. D. designed the experimental work, A. M. I. K. and G. L. designed the experimental work, analyzed the experiments and wrote the manuscript. All authors have read and agreed to the publication of this manuscript.

## Conflicts of interest

There are no conflicts to declare.

## Acknowledgements

The study was carried out at the expense of the Russian Science Foundation No. 22-13-00082, https://www.rscf.ru/en/project/22-13-00082/. The authors are grateful to the "Centre for Optical and Laser Materials Research", "Interdisciplinary Resource Centre for Nanotechnology" of St. Petersburg State University Research Park for technical support.

## References

1 K. Hüll, J. Morstein and D. Trauner, *Chem. Rev.*, 2018, **118**, 10710–10747.
2 W. A. Velema, W. Szymanski and B. L. Feringa, *J. Am. Chem. Soc.*, 2014, **136**, 2178–2191.
3 P. Kobauri, F. J. Dekker, W. Szymanski and B. L. Feringa, *Angew. Chem., Int. Ed.*, 2023, 62.
4 M. Kathan and S. Hecht, *Chem. Soc. Rev.*, 2017, **46**, 5536–5550.
5 M. Scheiner, A. Sink, P. Spatz, E. Endres and M. Decker, *ChemPhotoChem*, 2021, **5**, 149–159.
6 I. S. Shchelik, A. Tomio and K. Gademann, *ACS Infect. Dis.*, 2021, **7**, 681–692.
7 J. Broichhagen, I. Jurastow, K. Iwan, W. Kummer and D. Trauner, *Angew. Chem., Int. Ed.*, 2014, **53**, 7657–7660.
8 Y. Q. Yeoh, J. Yu, S. W. Polyak, J. R. Horsley and A. D. Abell, *ChemBioChem*, 2018, **19**, 2591–2597.
9 M. Wegener, M. J. Hansen, A. J. M. Driessen, W. Szymanski and B. L. Feringa, *J. Am. Chem. Soc.*, 2017, **139**, 17979–17986.
10 E. Alarcón, A. M. Edwards, A. Aspee, F. E. Moran, C. D. Borsarelli, E. A. Lissi, D. Gonzalez-Nilo, H. Poblete and J. C. Scaiano, *Photochem. Photobiol. Sci.*, 2010, **9**, 93–102.
11 B. Biscussi, V. Richmond, C. J. Baier, P. A. Mañez and A. P. Murray, *CNS Neurol. Disord.: Drug Targets*, 2020, **19**, 630–641.
12 D. A. Rodríguez-Soacha, M. Scheiner and M. Decker, *Eur. J. Med. Chem.*, 2019, **180**, 690–706.
13 M. Noetzli and C. B. Eap, *Clin. Pharmacokinet.*, 2013, **52**, 225–241.
14 K. R. Valasani, G. Hu, M. O. Chaney and S. S. Yan, *Chem. Biol. Drug Des.*, 2013, **81**, 238–249.
15 S. A. Grando, R. M. Horton, E. F. R. Pereira, B. M. Diethelm-Okita, P. M. George, E. X. Albuquerque and B. M. Conti-Fine, *J. Invest. Dermatol.*, 1995, **105**, 774–781.
16 X. Chen, S. Wehle, N. Kuzmanovic, B. Merget, U. Holzgrabe, B. König, C. A. Sotriffer and M. Decker, *ACS Chem. Neurosci.*, 2014, **5**, 377–389.
17 M. Scheiner, A. Sink, M. Hoffmann, C. Vrigneau, E. Endres, A. Carles, C. Sotriffer, T. Maurice and M. Decker, *J. Am. Chem. Soc.*, 2022, **144**, 3279–3284.
18 K. Horbatok, T. Makhnii, V. Kosach, V. Danko, A. Kovalenko, S. Fatiushchenkov, P. Borysko, I. Pishel, O. Babii, A. S. Ulrich, T. Schober, S. Afonin and I. V. Komarov, *J. Visualized Exp.*, 2023, 199.
19 L. Gao, J. C. M. Meiring, A. Varady, I. E. Ruider, C. Heise, M. Wranik, C. D. Velasco, J. A. Taylor, B. Terni, T. Weinert, J. Standfuss, C. C. Cabernard, A. Llobet, M. O. Steinmetz, A. R. Bausch, M. Distel, J. Thorn-Seshold, A. Akhmanova and O. Thorn-Seshold, *J. Am. Chem. Soc.*, 2022, **144**, 5614–5628.
20 V. A. Gutzeit, A. Acosta-Ruiz, H. Munguba, S. Häfner, A. Landra-Willm, B. Mathes, J. Mony, D. Yarotski, K. Börjesson, C. Liston, G. Sandoz, J. Levitz and J. Broichhagen, *Cell Chem. Biol.*, 2021, **28**, 1648–1663.e16.
21 R. Qazi, C. Yeon Kim, I. Kang, D. Binazarov, J. G. McCall and J. Jeong, *ChemPhotoChem*, 2021, **5**, 96–105.
22 Z. B. Mehta, N. R. Johnston, M.-S. Nguyen-Tu, J. Broichhagen, P. Schultz, D. P. Larner, I. Leclerc, D. Trauner, G. A. Rutter and D. J. Hodson, *Sci. Rep.*, 2017, **7**, 291.
23 J. A. Frank, M.-J. Antonini, P.-H. Chiang, A. Canales, D. B. Konrad, I. C. Garwood, G. Rajic, F. Koehler, Y. Fink and P. Anikeeva, *ACS Chem. Neurosci.*, 2020, **11**, 3802–3813.
24 H. Jung, S. You, C. Lee, S. You and Y. Kim, *Chem. Commun.*, 2013, **49**, 7528.
25 M. Villa, S. Angeloni, A. Bianco, A. Gradone, V. Morandi and P. Ceroni, *Nanoscale*, 2021, **13**, 12460–12465.

26 V. Arkhipova, H. Fu, M. W. H. Hoorens, G. Trinco, L. N. Lameijer, E. Marin, B. L. Feringa, G. J. Poelarends, W. Szymanski, D. J. Slotboom and A. Guskov, *J. Am. Chem. Soc.*, 2021, **143**, 1513–1520.
27 B. A. Kuzma, I. J. Pence, D. A. Greenfield, A. Ho and C. L. Evans, *Adv. Drug Delivery Rev.*, 2021, **177**, 113942.
28 Y. Wei, L. Kong, H. Chen, Y. Liu, Y. Xu, H. Wang, G. Fang, X. Shao, F. Liu, Y. Wang and Q. Chen, *Chem. Eng. J.*, 2022, **429**, 132134.
29 A. Motamarry, A. H. Negussie, C. Rossmann, J. Small, A. M. Wolfe, B. J. Wood and D. Haemmerich, *Int. J. Hyperthermia*, 2019, **36**, 816–825.
30 S. Jeong, D. A. Greenfield, M. Hermsmeier, A. Yamamoto, X. Chen, K. F. Chan and C. L. Evans, *Sci. Rep.*, 2020, **10**, 5360.
31 G. Bikbaeva, A. Pilip, A. Egorova, I. Kolesnikov, D. Pankin, K. Laptinskiy, A. Vervald, T. Dolenko, G. Leuchs and A. Manshina, *Nanomaterials*, 2023, **13**, 2409.
32 I. Kolesnikov, A. Khokhlova, D. Pankin, A. Pilip, A. Egorova, V. Zigel, M. Gureev, G. Leuchs and A. Manshina, *New J. Chem.*, 2021, **45**, 15195–15199.
33 D. Pankin, A. Khokhlova, I. Kolesnikov, A. Vasileva, A. Pilip, A. Egorova, E. Erkhitueva, V. Zigel, M. Gureev and A. Manshina, *Spectrochim. Acta, Part A*, 2021, **246**, 118979.
34 G. Bikbaeva, A. Egorova, N. Sonin, A. Pilip, I. Kolesnikov, D. Pankin, R. Borozn jak and A. Manshina, *ChemPhotoChem*, 2023, **7**, e202300131.
35 I. Kolesnikov, D. Mamonova, D. Pankin, G. Bikbaeva, A. Khokhlova, A. Pilip, A. Egorova, V. Zigel and A. Manshina, *Photochem. Photobiol.*, 2023, **99**, 929–935.
36 H.-L. Yang, L.-F. Bai, Z.-R. Geng, H. Chen, L.-T. Xu, Y.-C. Xie, D.-J. Wang, H.-W. Gu and X.-M. Wang, *Mater. Today Adv.*, 2023, **18**, 100376.
37 B. Zheng, J. Fan, B. Chen, X. Qin, J. Wang, F. Wang, R. Deng and X. Liu, *Chem. Rev.*, 2022, **122**, 5519–5603.
38 E. Hemmer, N. Venkatachalam, H. Hyodo, A. Hattori, Y. Ebina, H. Kishimoto and K. Soga, *Nanoscale*, 2013, **5**, 11339.
39 S. K. Gupta, K. Sudarshan and R. M. Kadam, *Mater. Today Commun.*, 2021, **27**, 102277.
40 I. E. Kolesnikov, A. V Povolotskiy, D. V Tolstikova, A. A. Manshina and M. D. Mikhailov, *J. Phys. D Appl. Phys.*, 2015, **48**, 075401.
41 B. Liu, C. Li, P. Yang, Z. Hou and J. Lin, *Adv. Mater.*, 2017, **29**, 1605434.
42 T. Jia and G. Chen, *Coord. Chem. Rev.*, 2022, **471**, 214724.
43 I. E. Kolesnikov, A. A. Kalinichev, M. A. Kurochkin, D. V Mamonova, E. Y. Kolesnikov, E. Lähderanta and M. D. Mikhailov, *Nanotechnology*, 2019, **30**, 145501.
44 I. E. Kolesnikov, D. V. Mamonova, M. A. Kurochkin, V. A. Medvedev and E. Y. Kolesnikov, *Phys. Chem. Chem. Phys.*, 2022, **24**, 27940–27948.
45 T. Higuchi, Y. Hotta, Y. Hikita, S. Maruyama, Y. Hayamizu, H. Akiyama, H. Wadati, D. G. Hawthorn, T. Z. Regier, R. I. R. Blyth, G. A. Sawatzky and H. Y. Hwang, *Appl. Phys. Lett.*, 2011, **98**, 071902.
46 A. V. Egorova, D. M. Egorov, N. O. Sonin, I. E. Kolesnikov, D. V. Pankin, A. A. Manshina and R. I. Baichurin, *Russ. J. Gen. Chem.*, 2022, **92**, 2191–2196.
47 I. E. Kolesnikov, D. V. Mamonova, M. A. Kurochkin, V. A. Medvedev and E. Y. Kolesnikov, *Ceram. Int.*, 2023, **49**, 20699–20705.